Heterogeneous Kinetics of N2O5 Uptake on Salt, with a Systematic Study of the Role of Surface Presentation (for N2O5 and HNO3)

ARTICLE *in* THE JOURNAL OF PHYSICAL CHEMISTRY · JANUARY 1996

Impact Factor: 2.78 · DOI: 10.1021/jp9503829

3 AUTHORS:

Frederick Frank Fenter
Frontiers Publishing
26 PUBLICATIONS **662** CITATIONS
SEE PROFILE

Francois Caloz
Diamoond SA
20 PUBLICATIONS **477** CITATIONS
SEE PROFILE

Michel J Rossi
Paul Scherrer Institut
259 PUBLICATIONS **6,495** CITATIONS
SEE PROFILE

Heterogeneous Kinetics of N_2O_5 Uptake on Salt, with a Systematic Study of the Role of Surface Presentation (for N_2O_5 and HNO_3)

Frederick F. Fenter, François Caloz, and Michel J. Rossi*

Laboratoire de Pollution Atmosphérique et Sol, Swiss Federal Institute of Technology, 1015 Lausanne, Switzerland

Received: February 9, 1995; In Final Form: October 12, 1995[⊗]

The kinetics for the uptake of N_2O_5 with NaCl [$N_2O_5(g) + NaCl(s) \rightarrow ClNO_2(g) + NaNO_3(s)$ (reaction 1)] and KBr[$N_2O_5(g) + KBr(s) \rightarrow$ products (reaction 6)] have been studied in a Teflon-coated Knudsen reactor. The product of reaction 1 is found to be $ClNO_2$, in agreement with previous studies. The only bromine-containing gaseous product observed for reaction 6 is Br_2; we propose a redox reaction in which Br^- is oxidized to molecular bromine with the concurrent formation of nitrite. The hypothesis is supported by the observation of nitrous acid in the product spectrum of reaction 6. The observed uptake coefficients are found to *depend strongly* on the total external surface area of the salt substrates, prepared by a number of methods. With samples of well-defined total external surface, we are able to determine the following values for the uptake coefficient: $\gamma_1 = (5.0 \pm 2.0) \times 10^{-4}$; $\gamma_6 = (4.0 \pm 2.0) \times 10^{-3}$. The values are smaller than previously reported. The unexpected dependence of the uptake kinetics on the surface presentation led us to conduct further experiments on the HNO_3 reaction with salt: $HNO_3(g) + NaCl(s) \rightarrow HCl(g) + NaNO_3(s)$ (reaction 2). From our new experiments conducted on various substrates, we find $\gamma_2 = (2.0 \pm 1.0) \times 10^{-2}$, in good agreement with our previous measurements on salt powder. The validity of calculating correction factors for the uptake coefficients, as recently proposed by Keyser and co-workers, is discussed in detail, and specific experimental tests of the theory are described. The role of internal surfaces in the overall observed uptake kinetics for the reactions of N_2O_5 is found to be remarkably well described by the treatment given by Keyser and co-workers. Additional experiments on the uptake kinetics of nitric acid, however, cast doubt that this treatment can be generally extended to all species of atmospheric interest. The atmospheric implications of these findings are discussed briefly.

1. Introduction

The reactions of the oxides of nitrogen, including nitric acid, with salt are now recognized to play a significant role in atmospheric chemistry.[1,2] Efforts to better characterize these processes are currently underway and include field studies,[3−5] laboratory measurements,[2,6−16] and atmospheric modeling.[17−23] Several species in the nitrate family have been proposed as potential reactants with atmospheric salt aerosols, including N_2O_5, HNO_3, $ClONO_2$, and NO_2. The reactions of these species with NaCl are characterized by a displacement of chloride for nitrate in the condensed phase with a release of a corresponding chlorine-containing volatile species:[24]

reaction		ΔH_r° (kJ mol^{-1})[25]
$N_2O_5(g) + NaCl(s) \rightarrow NaNO_3(s) + ClNO_2(g)$	(1)	−55.4
$HNO_3(g) + NaCl(s) \rightarrow NaNO_3(s) + HCl(g)$	(2)	−14.0
$ClONO_2(g) + NaCl(s) \rightarrow NaNO_3(s) + Cl_2(g)$	(3)	−79.7
$2NO_2(g) + NaCl(s) \rightarrow NaNO_3(s) + ClNO(g)$	(4)	−71.35

The implications for the release of gaseous, photolyzable chlorine species in both the troposphere and stratosphere have been a recent concern. In laboratory studies, uptake coefficients (γ), defined as the probability that a collision between the gaseous molecule and the solid results in the irreversible loss of the reactant from the gas phase, have been recently determined for each of these reactions. It is now generally recognized that reaction 4 is too slow to compete with reactions 1 and 2 in the atmosphere.[8] Reaction 3 may play a role in the regions of the atmosphere where $ClONO_2$ concentrations are elevated and where salt aerosol is present, for example in the stratosphere after volcanic eruption[5,23] or in the marine atmosphere in contact with sources of pollution. Timonen et al. have recently reported[13] that $\gamma_3 = 5.0 \times 10^{-3}$.

Reaction 1 has been studied in detail as a function of relative humidity on salt aerosol and as a function of chloride concentration in solution by Behnke and co-workers.[14,15] They find that the uptake probability on salt aerosol can be described by $\gamma = 3.0 \times 10^{-2}$ from 72 to 97% relative humidity, although the fraction of N_2O_5 that hydrolyzes to HNO_3 increases at the higher humidities. Livingston and Finlayson-Pitts have studied the reaction of N_2O_5 with dry NaCl powder,[12] concluding that $\gamma > 2.5 \times 10^{-3}$. Recently, Msibi et al. have carried out experiments on reaction 1 in an annular reactor based on denuder technology.[16] They analyze the axial deposition of nitrate produced from the hydrolysis of N_2O_5 in the presence of solid NaCl with 45−97% relative humidity. They conclude that the reaction probability is about 1×10^{-3} for the solid salt over this range of relative humidities. Thus, previous studies have found that the uptake coefficient for the reaction on sodium chloride below its deliquescence point is on the order of 10^{-3}, independent of the relative humidity.

The extent to which reactions 1 and 3 contribute to the displacement of chloride in salt aerosols will depend on the relative reactivity of nitric acid. Two recent studies on reaction 2 are in disagreement by about a factor of 100 for γ; we recently reported[2] that the uptake of HNO_3 on salt powders could be characterized by the large value of $\gamma = (2.8 \pm 0.5) \times 10^{-2}$, while Laux et al.[6] estimate a value of 5.0×10^{-4} on the basis of the rate of nitrate formation on a NaCl single crystal under

* Author to whom correspondence should be directed.
[⊗] Abstract published in *Advance ACS Abstracts,* December 15, 1995.

0022-3654/96/20100-1008$12.00/0

similar experimental conditions of temperature and pressure. The reason for the discrepancy is not obvious, but the matter needs to be resolved if we are to better assess the relative roles of reactions 1−4 in the earth's atmosphere.

The reactivity of N_2O_5 with respect to bromides is poorly characterized and may also represent a source of photolyzable bromine compounds in the atmosphere. Finlayson-Pitts et al.[24] have reported the formation of $BrNO_2$ in the reaction with NaBr, suggesting that the mechanism is analogous to that of the chloride:

$$N_2O_5(g) + NaBr(s) \rightarrow BrNO_2(g) + NaNO_3(s) \qquad (5)$$

If this is indeed the stoichiometry, then the reaction may represent an important source of bromine atoms in the marine boundary layer.

In this report, we describe direct kinetic measurements of the uptake of N_2O_5 on salt using a low-pressure flow reactor. Although a few experiments are reported for the interaction with NaBr, the two salts selected for detailed study are NaCl and KBr:

$$N_2O_5(g) + KBr(s) \rightarrow \text{products} \qquad (6)$$

Our principle goals are to determine the uptake coefficients for N_2O_5 on NaCl and KBr, to identify the products of the reaction, and to quantify their yields.

In this study, we make an effort to understand the effect of internal surface area on the observed value of the uptake coefficient. This approach is necessary due to the recent conclusions reached by Keyser and co-workers,[26−28] who claim that the use of "porous" solid substrates (i.e., those that contain a non-negligible internal void) must entail the application of large correction factors to obtain the true uptake coefficient from the observed. We discuss experiments designed to test this hypothesis directly, both for the N_2O_5 reactions detailed above and for the reactions of HNO_3 with NaCl and KBr:

$$HNO_3(g) + NaCl(s) \rightarrow HCl(g) + NaNO_3(s) \qquad (2)$$

$$HNO_3(g) + KBr(s) \rightarrow HBr(g) + KNO_3(s) \qquad (7)$$

The results will be discussed in terms of the applicability of the correction-factor calculation as outlined by Keyser and co-workers and in terms of the relative importance of reactions 1−7 in the chemistry of the atmosphere.

2. Experimental Details

The experiments were carried out using the Knudsen reactor shown schematically in Figure 1. The use of these reactors has been described in detail elsewhere,[29,30] and the specific experimental apparatus has been recently presented in the literature.[2] Here we give only a brief account of the operation. The characteristics of the reactor are summarized in Table 1.

The apparatus is comprised of three basic parts—the vacuum line with gas inlets, the reactor, and the detection system. The gas-handling installation includes a calibrated volume monitored by a 100-mbar pressure transducer (MKS Baratron), with which absolute flow calibrations can be carried out. The gas-phase reactant is introduced into the reactor in two ways: (1) as a known flow through a capillary or (2) via a pulse across a small solenoid valve (General Valve, Series 9), opened typically for 1 ms. The pulse-to-pulse reproducibility of the valve is about 10% for the short durations employed. Control experiments and kinetic measurements are conducted under identical conditions by use of the isolation plunger, which seals the solid

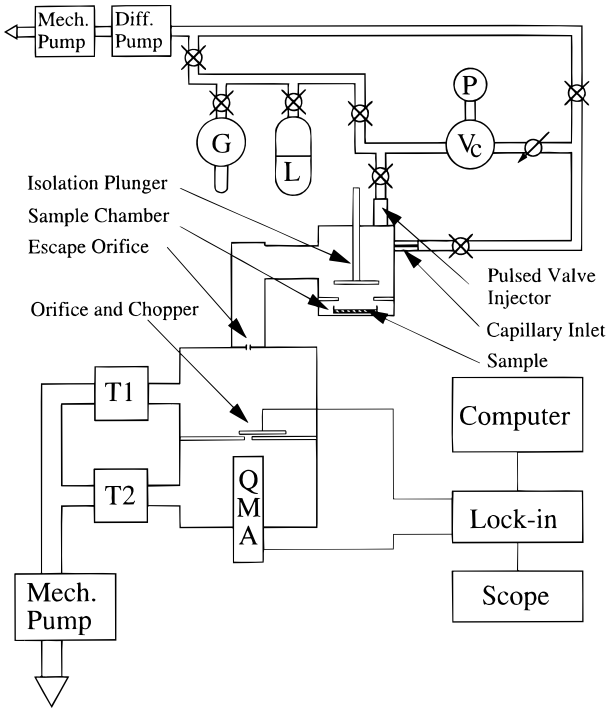

Figure 1. Schematic drawing of the experimental apparatus: G, gas sample; L, liquid sample; P, pressure gauge; V_c, calibrated volume; T1 and T2, turbomolecular pumps; QMA, mass spectrometer.

TABLE 1: Knudsen-Cell Parameters

reactor parameter	value
volume	1830 cm^3
surface area (total)	2000 cm^2
gas number density	$(1-1000) \times 10^{10}$ cm^{-3}
sample collision frequency[a]	$\omega = 2.0\, A_h\, (T/M)^{0.5}$ s^{-1}
orifice diameters	4 mm, 8 mm, 9 mm
escape rate constant ($\phi = 9$ mm)[a]	$1.02(T/M)^{0.5}$ s^{-1}
escape rate constant ($\phi = 4$ mm)[a]	$0.21(T/M)^{0.5}$ s^{-1}

[a] A_h, the sample surface area, is typically on the order of 10 cm^2. [b] Values determined directly by experiment.

sample from the gaseous reactant. The reactor is operated in the molecular flow regime, and the characteristic residence time and density of gas-phase species in the Knudsen cell are set by the escape-orifice diameter. All internal surfaces of the reactor are coated with Teflon to minimize unwanted heterogeneous processes.

The reactor is positioned on a vacuum chamber evacuated by two turbomolecular pumps. The effusive beam which is formed at the exit orifice of the cell is chopped by a tuning fork at 145 Hz before passing into the ionization volume of a quadrupole mass spectrometer (Balzers model QMG 421), mounted in the second stage of the differentially pumped vacuum chamber. The modulated electron multiplier signal is processed by a digital lock-in amplifier (Stanford Research SR830 DSP) and transferred directly to a personal computer for storage and analysis. The mass spectrometer signal measures directly the gas flow leaving the reactor.

The salt samples are occasionally heated under vacuum before the experiment to remove adsorbed water. For this we employed a heatable sample holder, the design of which will be described in detail elsewhere. Briefly, it consists of a resistively-heated nickel-coated copper support, attached to a water-cooled flange via a tapered knife edge. Thermal conduction between the support and the sample is assured by a thin layer of gallium. With this support, samples are routinely heated under vacuum up to 550 K.

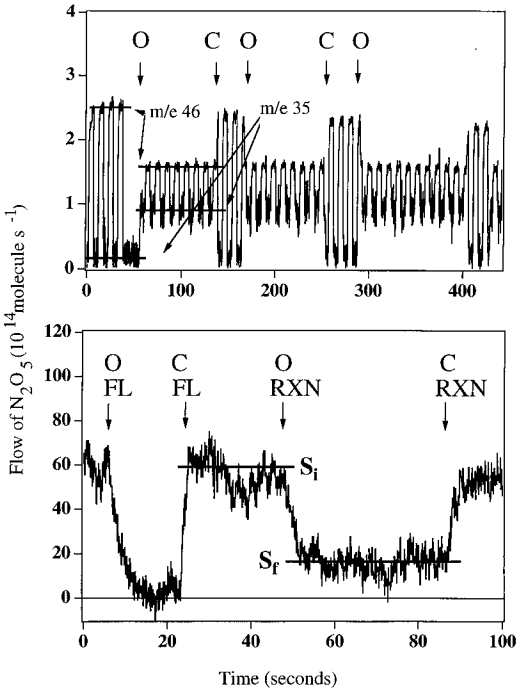

Figure 2. Examples of N_2O_5 + NaCl steady-state experiments. The letters O and C refer to the opening and closing of the sample chamber; on the bottom, FL and RXN refer to manipulations of the flow and isolation plunger. In the top frame, *m/e* (NO_2^+) and *m/e* 35 (Cl^+) are followed to separate the *m/e* 46 contribution due solely to N_2O_5. The experiment is conducted with an 8-mm orifice under small flow conditions. In the bottom frame, *m/e* 62 (NO_3^+) is monitored in an experiment conducted using the reactor described in ref 2 ($k_{esc} = 0.7$ s^{-1} for N_2O_5; $\omega = 64$ s^{-1}). Steady-state analysis of this experiment yields $\gamma = 3.0 \times 10^{-2}$, in good agreement with the *m/e* 46 results.

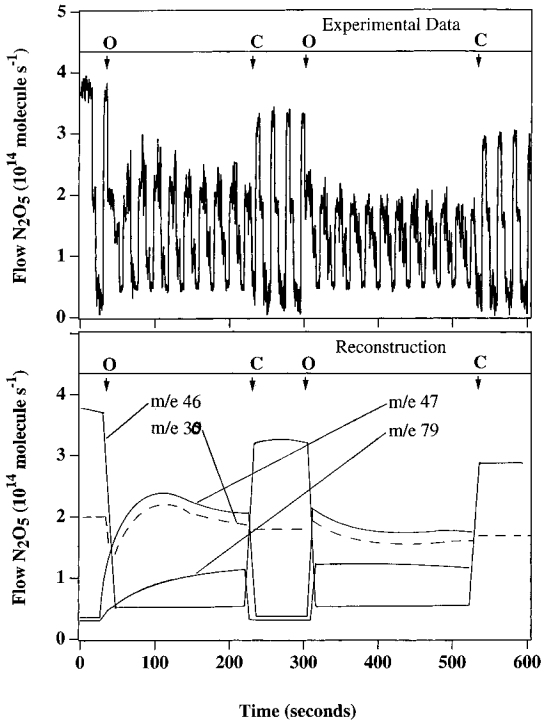

Figure 3. Example of the N_2O_5 + KBr steady-state experiment. Here the following masses are monitored: *m/e* 46 (NO_2^+), *m/e* 30 (NO^+), *m/e* 47 ($HONO^+$), and *m/e* 79 (Br^+); the last two are amplified by a factor of 10. A schematic reconstruction of the experiment is provided in the bottom frame to facilitate interpretation. See text for details and analysis. The experiment is conducted with an 8-mm orifice under small flow conditions.

(a) Experimental Protocol. We use the apparatus in two distinct modes, referred to here as *steady-state* and *pulsed-valve* experiments. Below, we briefly describe the procedure for each; a more detailed account has been previously published.[2]

In the steady-state experiment, a known constant flow of the gas-phase reactant is introduced into the reactor via a capillary with the plunger closed to isolate the solid sample. Because the only loss term is the rate of effusion out of the cell, the density of the reactant can be precisely determined by solving for the steady-state concentrations. At the moment that the plunger is opened, the density of the gaseous reactant will decrease if there is an interaction between the gas-phase species and the solid, i.e., an uptake. Once the new steady state is reached, we can describe the first-order rate of uptake, k^I, in terms of the rate of effusive loss from the cell, k_{esc}, and the change in mass spectrometer signal:

$$k^I = \left(\frac{S_i}{S_f} - 1\right) \cdot k_{esc} \qquad \text{(eq 1)}$$

where S_i and S_f are the mass spectrometer steady-state signals before and during the reaction, respectively. The application of this equation requires that the uptake process be first order with respect to the gas-phase density, which can be verified by showing that the observed rate of uptake is independent of the reactant flow rate. The value of k_{esc} is determined directly in a control experiment. Experimental traces of steady-state experiments conducted on NaCl and KBr are found in Figures 2 and 3.

In the pulsed-valve experiments, the solenoid valve is opened for a brief period, typically 1 ms, to introduce the reactant. The flux of all gaseous species from the cell is monitored in real time by the mass spectrometer. A control experiment, in which the solid sample is isolated by the plunger, yields a simple exponential decay of the reactant signal that corresponds to the appropriate value of k_{esc}. Then the plunger is opened, and a second pulse is actuated. From the resulting decay trace, the first-order rate of uptake is directly determined by fitting to a simple exponential decay function. Examples of pulsed-valve experiments for NaCl and KBr can be found in Figure 4.

(b) Preparation of Salt Substrates. Salt grains are nonporous; i.e., the total exposed surface (as measured by the BET technique)[13] is equivalent to the geometrical surface area of the grains. Therefore, the total exposed surface of a sample can be calculated (for the sieved grains) or estimated (for powders) from microscope or scanning-electron-microscope (SEM) images, with which the typical grain size and the grain size distribution can be determined. As discussed below, SEM images are also used to assess the exposed surface of spray-deposited samples. We thus rely on microscope images to evaluate the surface area presented by the samples, using the assumption (confirmed in other laboratories) that the material studied is nonporous.

(1) Single-Crystal Spectroscopic-Grade Flats. Windows for IR spectroscopy of NaCl and KBr (ϕ = 50mm, Bicron Corporation) were employed as reactive surfaces, presented either as polished or depolished. The polished surfaces are prepared by gliding a sheet of wet optical paper over the surface and then allowing it to dry. The salt flats are depolished by gentle rubbing with fine-grained sandpaper with careful subsequent elimination of surface powder (by rinsing with solvents or by blowing with pressurized CO_2). Before each experiment, the cell windows are typically heated to 450 K for several hours under vacuum to eliminate adsorbed water. With the mass spectrometer, the quantity of desorbing water can be continually

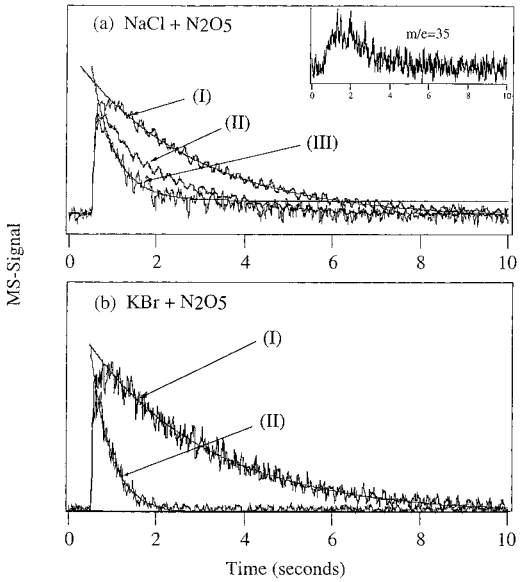

Figure 4. Pulsed valve experiments conducted for reactions 1 and 6, each showing the result of the injection of 5×10^{14} molecules of N_2O_5. For both experiments, the gas-sample collision rate was 43 s^{-1}. In part a, pulse (I) shows the *m*/*e* 46 signal after introduction of N_2O_5 with the sample chamber closed. The resulting decay of 0.35 s^{-1} corresponds to the known k_{esc} for the 8-mm-diameter orifice. Pulse (II) is actuated under the same conditions with the isolation plunger open; the resulting decay is nonexponential due to the formation of $ClNO_2$. When pulse (II) is corrected for the real-time contribution of $ClNO_2$ (determined in a separate experiment by following *m*/*e* 35 under the same conditions, shown in the inset), curve (III) is obtained. The first-order decay constant for curve (III) is 1.6 s^{-1}, in good agreement with the value determined by the steady-state technique. In part b, the situation is simplified because the products of the reaction do not contribute to *m*/*e* 46. The reactive pulse is fit directly by an exponential decay function to obtain the first-order rate of 2.2 s^{-1} for the N_2O_5 uptake.

monitored, and complete drying is assured by heating the substrate until the water signal decreases to its background level.

(2) Spray-Deposited Samples. We have coated 50-mm-diameter quartz and glass optical flats using a capillary-source atomizer to obtain a polycrystalline sample whose total exposed surface is nearly equivalent to the area of the coated flat, as determined from analysis of SEM images. Methanol or water is saturated with the salt of interest, and a fine spray of the solution is deposited on the optical flat heated to the temperature of 400 K. The coatings of the highest quality are obtained using methanol. Typically, 1−5 mg of salt can be evenly deposited onto the quartz support with coverage approaching 100%, resulting in an average thickness of less than 2 μm. The samples are routinely analyzed by an optical microscope and a profilometer (Tencor Alpha-step 200) to determine the total coverage and by a scanning electron microscope to ascertain the quality of the coating (see Figure 5).

(3) Monodisperse Sub-millimeter Grain. High-purity salt is available as grain in the sub-millimeter size range from Fluka. This salt is sieved for various size fractions to obtain monodisperse grain with a narrow size distribution. The samples thus prepared are characterized by a non-negligible and well-characterized total exposed surface area, allowing us to study the effect of this parameter on the observed overall uptake kinetics.

(4) Finely Ground Powders. In some experiments, powders are used as the substrate. The samples are prepared by grinding in a ball mill and then sieving to isolate the desired fraction. For the powder employed in the product study, we collected the 35−160 μm grain. For other experiments, the sieve fraction

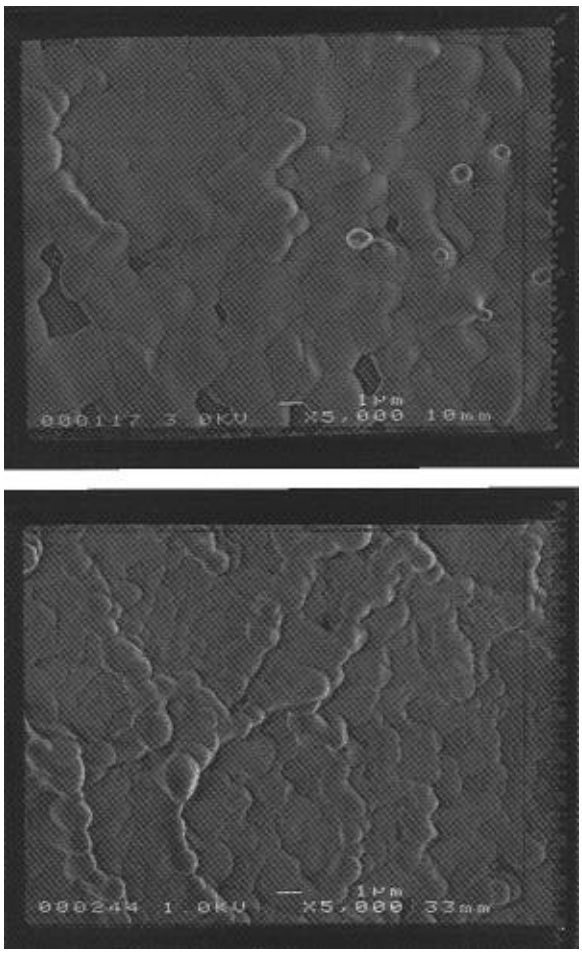

Figure 5. Scanning electron microscope images of the methanol spray-deposited substrates used in this study. The full horizontal scale is 20 μm. The images demonstrate the lack of internal surface area when methanol is employed as the atomizing solvent: In part a (top) and part b (bottom), typical KBr and NaCl surfaces are shown, respectively.

of $\phi < 25$ μm is used. The total exposed surface area of these samples is relatively large and difficult to characterize precisely because the grain-diameter distribution can only be estimated from microscope images.

(c) Preparation of Gas-Phase Compounds. Dinitrogen pentoxide (N_2O_5) is prepared by the oxidation of NO_2 with excess ozone. The O_3/O_2 mixture that evolves from an ozonator is passed through a P_2O_5 trap (to eliminate residual moisture) before being mixed with dried NO_2. The N_2O_5 is collected in a methanol/dry-ice bath (195 K) and is subsequently analyzed for purity by IR spectroscopy and by mass spectroscopy. Once the inlet capillary is passivated, very little N_2O_5 is hydrolyzed during injection into the reactor. The HNO_3 impurity is assessed *in situ* by mass spectrometry before each experiment under the exact conditions of the experiment by comparing the low-intensity *m*/*e* 63 peak of HNO_3 to the low-intensity *m*/*e* 62 peak of N_2O_5. We use the result of our measurements that the contribution of HNO_3 at *m*/*e* 62 is on the order of 1% of the intensity of the *m*/*e* 63 peak so that both HNO_3 and N_2O_5 may each be monitored separately without ambiguity. Both signals are mass-flow calibrated, and we determine that the nitric acid impurity is on the order of 1%. Mass spectrometric data are summarized in Figure 6. The spectra may change to a small extent over time, especially for the nitrogen oxides, for which the instrument response is not perfectly stable over the course of weeks. However, calibrations are performed routinely to insure that the relationship between mass spectrum intensity and flow rate of the species of interest is known.

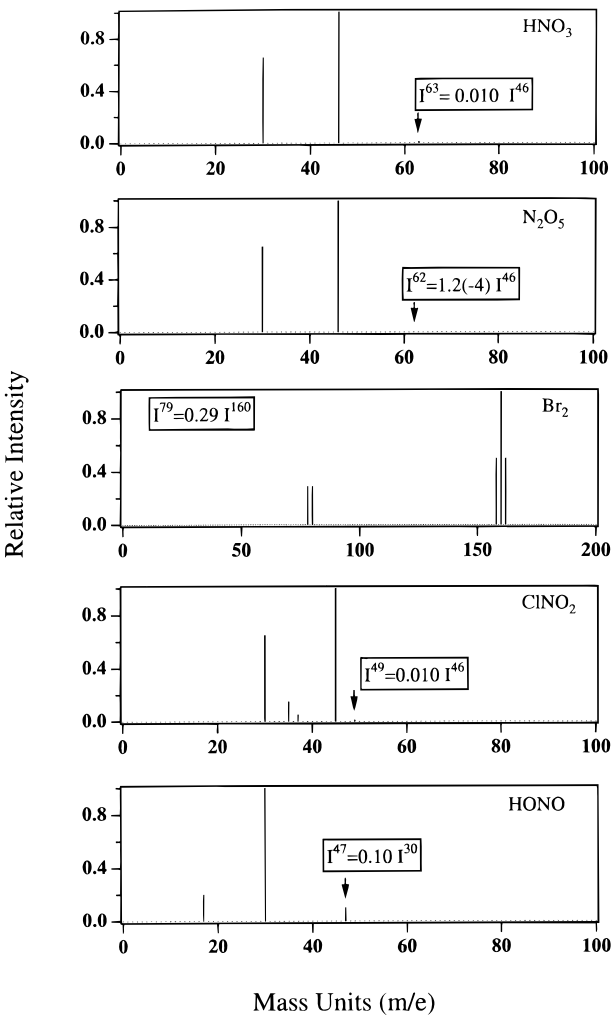

Figure 6. Summary of the mass spectrometric data determined and employed in this study. Arrows identify peaks too weak to be seen on this scale. The spectra are included to facilitate the reader's interpretation of the experiments.

In order to calibrate production yields of the studied reactions, we obtained a sample of Br_2 and synthesized $ClNO_2$ according to the procedure of Ganske et al.[31] Briefly, HCl gas is passed through a mixture of fuming sulfuric and nitric acids, and the evolving gases are collected in a liquid nitrogen cooled trap. The liquid is twice distilled to eliminate molecular chlorine and nitric acid. Then N_2O_5 is added to the resulting impure $ClNO_2$ to oxidize trace ClNO. The resulting sample is doubly distilled a second time to obtain purified $ClNO_2$. The mass spectrum of the $ClNO_2$ thus obtained is shown in Figure 6.

3. Results

We begin this section with a discussion of experimental uncertainty. Most of the experiments described below are conducted in the steady-state configuration. Typically, for a given set of experimental conditions, the measured values are distributed about the mean with a standard deviation of 5−10% (c.f. Figure 7). From the results presented below, it will be obvious that the systematic error (due to such effects as surface roughness) is the dominant source of uncertainty and that this error is not easily assessed. The uncertainties are assigned in the following manner: (1) If several experiments are conducted under nominally identical conditions, the quoted uncertainty is the 2σ statistical limit associated with the average. (2) If a single or few (≤ 3) experiments are conducted, a minimum uncertainty of 20% is assigned. (3) If the experiment is designed to measure the true uptake coefficient directly, we add 30% uncertainty. The additional uncertainty is needed to take into account potential systematic error due to surface preparation.

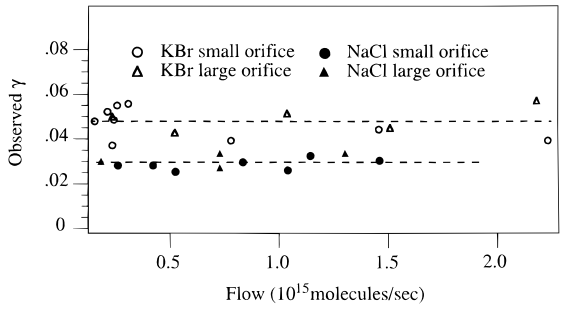

Figure 7. Plot of the observed values of the uptake coefficient as a function of the N_2O_5 flow for reactions 1 and 6 and for the two orifices employed in this study. The substrate is powder sieved for the fraction $160 < \phi < 35$ μm. The independence of the initial rate of uptake over several orders of magnitude in N_2O_5 density is strong evidence that the process is first order with respect to N_2O_5 concentration.

(a) Salt-Powder Study. Our initial investigation of the N_2O_5 reaction with NaCl and KBr involved the use of powder substrates. The experiments shown in Figures 2 and 3 show typical results for the NaCl and KBr, respectively, reactions with N_2O_5. In most experiments, we follow the *m*/*e* 46 signal to follow the N_2O_5 density, but a few were carried out using *m*/*e* 62 (NO_3^+). An example of the latter is given in Figure 2. The good agreement between the results for the experiments conducted at *m*/*e* 62 and *m*/*e* 46 provides an important confirmation that HNO_3 is absent under our experimental conditions and therefore did not interfere with the N_2O_5 kinetic measurements. Once this was established, we routinely monitored N_2O_5 at the more sensitive *m*/*e* 46 peak of its mass spectrum. We continued to monitor the quality of different batches of N_2O_5 by regularly recording *m*/*e* 62 (for N_2O_5) and 63 (indicative of HNO_3).

Upon exposure of N_2O_5 to NaCl, we observe that the *m*/*e* 46 signal decreases and that new peaks appear at *m*/*e* 35 (Cl^+), *m*/*e* 36 (HCl^+), and *m*/*e* 49 (ClN^+), with their associated ^{37}Cl signals. The small amount of HCl (<5% molar yield) is probably formed indirectly via the hydrolysis of N_2O_5 by trace humidity, with the resulting HNO_3 displacing chloride via reaction 2 to form HCl. In a separate experiment, we confirmed that $ClNO_2$ is not hydrolyzed to HCl on salt under our experimental conditions. The ratio of the *m*/*e* 35 and *m*/*e* 49 product signals is identical to that for the laboratory-prepared, authentic sample of $ClNO_2$. Our observations are consistent with the conclusions of previous studies that $ClNO_2$ is the principal chlorine-containing gas-phase product of the reaction. Because we follow *m*/*e* 46 to monitor the uptake of N_2O_5, the signal during reaction has to be corrected for the presence of $ClNO_2$. In each experiment the *m*/*e* 35 intensity is recorded, with which the $ClNO_2$ contribution to *m*/*e* 46 can be calculated by referring to the mass spectrum of the authentic sample. On the basis of the mass flow calibrations we carried out for $ClNO_2$ and for N_2O_5, we conclude that the yield of $ClNO_2$ is (60 ± 6)% relative to the number of N_2O_5 molecules taken up by the NaCl powder, where the estimated error is determined by the uncertainty of the mass flow calibrations of N_2O_5 and $ClNO_2$. Mass spectra recorded during the reaction reveal no additional products.

The interaction of N_2O_5 with NaCl powder is studied as a function of flow rate and escape-orifice diameter. The results are summarized in Figure 7, where it can be seen that the rate of uptake remains independent of the initial N_2O_5 flow, varied

TABLE 2: Experimental Results: NaCl + N_2O_5

substrate	γ_{obs} ($\times 10^{-3}$)	expts	corr fac[a]	γ_{tr} ($\times 10^{-3}$)[b]
(1) powder (35−160 μm)[c]	30 ± 5.0	20	32	0.9
(2) grain (400 μm)[d]	6.0−29	4	4.7−22	2.0
(3) grain (200 μm)[e]	13−32	3	10−27	2.0
(4) spray-coated sample (MeOH)	0.5 ± 0.2	3		0.5
(5) polished window face	<0.1	2		<0.1
(6) depolished window face	0.4 ± 0.2	2		0.4

[a] Calculated using equations from Table 5. [b] See text for discussion of uncertainty. The recommended value cited in the text weighs most heavily the results for substrates 4 and 6. [c] Grain diameter taken as 50 μm; ρ_{bulk} = 1.2 g cm^{-3}. [d] Sieve fraction between 500 and 250 μm. [e] Sieve fraction between 250 and 160 μm.

between (0.5 and 63) $\times$ 10^{14} cm^{-3}, confirming the first-order kinetic rate law for this process. The value for the uptake coefficient on NaCl powder is (3.0 ± 0.6) $\times$ 10^{-2}. The results of all the kinetic measurements for reaction 1 are summarized in Table 2.

In Figure 4a we show the same interaction in real time after a pulsed introduction of N_2O_5 through the solenoid valve. As before, *m*/*e* 35 is monitored in a subsequent experiment to separate the *m*/*e* 46 signal of N_2O_5 from that of $ClNO_2$. The control pulse (sample isolated) yields the appropriate value for k_{esc}, the rate of effusive loss of N_2O_5 from the reactor. It is seen in Figure 4a that the N_2O_5 signal trace in the presence of NaCl is not a simple exponential decay because of the *m*/*e* 46 contribution of the $ClNO_2$ product. With the *m*/*e* 35 signal trace (shown in the inset), the observed profile can be corrected for product formation, and the corrected decay trace yields a first-order rate constant in good agreement with that obtained in the steady-state study.

Guided by the only previous study of the reaction of a bromide with N_2O_5, where it was determined that $BrNO_2$ is formed as a principal product,[24] we anticipated the following process for reaction 6:

$$N_2O_5(g) + KBr(s) \rightarrow BrNO_2(g) + KNO_3(s) \qquad (6a)$$

Gaseous $BrNO_2$ is not sufficiently stable to permit the synthesis of a sample for mass spectrometric calibration.[34] However, the mass spectrum of $BrNO_2$, formed via reaction 6a, has been observed to have intense peaks at *m*/*e* 46 (NO_2^+) and *m*/*e* 79 (Br^+), with a weak signal at *m*/*e* 93 (BrN^+).[24] Our observations from the steady-state experiments, an example of which is shown in Figures 2 and 3, can be summarized as follows: (1) The *m*/*e* 46 signal decreases upon exposure of NaBr or KBr powder to N_2O_5, and this response is independent of the flow and k_{esc}, indicating that the detected products do not significantly contribute to the NO_2^+ peak at *m*/*e* 46. Unlike for reaction 1, we can use the uncorrected *m*/*e* 46 signal to directly monitor the N_2O_5 density during the reaction. (2) No signal is observed at *m*/*e* 93 or *m*/*e* 95; i.e., no BrN^+ fragment is observed. (3) A strong signal is observed at *m*/*e* 79 and *m*/*e* 81 (Br^+) and at *m*/*e* 158, *m*/*e* 160, and *m*/*e* 162 (Br_2^+). The relative strengths of Br_2^+ and Br^+ mass signals in the product spectrum are identical to that for the pure Br_2 sample, from which we conclude that Br_2 is the only gas-phase bromine-containing species formed under our experimental conditions. From the mass flow calibrations of Br_2 and N_2O_5, we determine that the product is formed with (35 ± 5)% molar yield. (4) The product spectrum shows additional new intensity at *m*/*e* 17 (OH^+), *m*/*e* 30 (NO^+), and *m*/*e* 47 ($HONO^+$). (5) N_2O_5 reacts with higher uptake probability on KBr powder than for the corresponding

TABLE 3: Experimental Results: KBr + N_2O_5

substrate	γ_{obs} ($\times 10^{-3}$)	expts	corr fac[a]	γ_{tr} ($\times 10^{-3}$)[b]
(1) powder (35−160 μm)[c]	55 ± 10	20	15.4	3.5
(2) powder (<10 μm)[d]	98 ± 20	3	16.1	6.0
(3) grain (300 μm)[e]	25−58	4	5.7−14.4	4.0
(4) grain (200 μm)[f]	23−60	4	6.4−14.3	4.0
(5) spray-coated sample (H_2O)[g]	0.5.−80	8		
(6) spray-coated sample (MeOH)	3.0 ± 1.5	6		3.0
(7) polished window face	<0.1	1		<0.1
(8) depolished window face	4.0 ± 1.0	2		4.0

[a] Calculated from equations given in Table 5. [b] See text for discussion of uncertainty. The recommended value in the text weighs most heavily the experiments conducted on substrates 6 and 8. [c] Grain diameter taken as 50 μm; ρ_{bulk} = 1.4 g cm^{-3}. [d] Grain diameter taken as 5 μm; ρ_{bulk} = 1.25 g cm^{-3}. [e] Sieve fraction between 500 and 250 μm; SEM image shows ϕ = 300 μm. [f] Sieve fraction between 250 and 160 μm. [g] Systematic dependence on the coating thickness.

NaCl reaction, obtaining γ_6 = (5.5 ± 1.0) $\times$ 10^{-2}. All the kinetic results for reaction 6 are summarized in Table 3.

Our observations suggest that $BrNO_2$, if formed in an initial interaction between N_2O_5 and KBr, is not stable with respect to subsequent reaction with the bromide:

$$N_2O_5(g) + KBr(s) \rightarrow KNO_3(s) + BrNO_2(ads) \qquad (6a)$$

$$BrNO_2(ads) + KBr(s) \rightarrow KNO_2(s) + Br_2(g) \qquad (8)$$

HONO is produced by the reaction of nitrite with nitric acid, the latter originating from the hydrolysis of N_2O_5:

$$N_2O_5(g) + H_2O(ads) \rightarrow 2HNO_3(ads) \qquad (9)$$

$$HNO_3(ads) + KNO_2(s) \rightarrow KNO_3(s) + HONO(g) \qquad (10)$$

Mass spectral information for HONO can be obtained by reacting HNO_3 with $NaNO_2$ in the Knudsen reactor. The experiment is carried out in the steady-state mode with a flow of approximately 10^{15} molecule s^{-1} of HNO_3. The uptake of HNO_3 on $NaNO_2$ powder is followed at *m*/*e* 63 and is found to be extremely efficient ($\gamma > 0.1$). The product of the acidification of nitrite is HONO, as given by reaction 10. We record the changes at *m*/*e* 30 (NO^+), *m*/*e* 46 (NO_2^+), *m*/*e* 47 ($HONO^+$), and *m*/*e* 63 (HNO_3^+) before and during the exposure of HNO_3 to $NaNO_2$. When the sample is exposed to HNO_3, the *m*/*e* 46 and 63 signals decrease to low levels, the *m*/*e* 30 signal increases, and new intensity appears at *m*/*e* 47. Once the residual HNO_3 contribution is subtracted, on the basis of the *m*/*e* 63 intensity, the mass spectrum for HONO is determined; in particular, we find that the *m*/*e* 30 signal is a factor of 10 ± 2 larger than its *m*/*e* 47 peak, as summarized in Figure 6. This result is entirely in accord with the conclusion that the *m*/*e* 30 and *m*/*e* 47 signals observed in the product spectrum of the N_2O_5 + KBr reaction are due to HONO (c.f. Figure 2).

In addition, the gas-phase product responsible for the *m*/*e* 47 peak is found to have a molecular weight of 50 ± 10 amu by the following experiment: Reaction 6, once underway, is stopped by lowering the plunger, thus isolating the sample from the HNO_3 flow, and the decay of the *m*/*e* 47 signal is measured. This directly yields the rate of effusive loss for the species responsible for the signal, which in turn can be used to calculate the molecular weight via the appropriate equation given in Table 1. A final test of the HONO formation hypothesis can be carried out by rigorously drying the bromide before the experiment. Under dry conditions, the nitrite intermediate should remain in

the condensed phase. The salt sample, present on a thickly-coated spray-deposited glass flat, is heated under vacuum with the use of the heatable sample holder. When this procedure is carried out, we find that molecular bromine is still formed as a product but that the *m/e* 47 (HONO) signal is no longer present. This is additional, indirect evidence for the proposed mechanism.

(b) Substrates of Limited Total Reactive Surface. *(1) Window Faces.* To test the extent to which underlying layers in grain or powder samples contribute to the observed rate of N_2O_5 uptake, we studied the reactions on spectroscopy grade salt flats. For reactions 1 and 6, no uptake ($\gamma < 10^{-4}$) is observed if the window face is polished by the procedure outlined in the Experimental Section. With a slightly depolished window, however, an interaction is observed. These experiments are conducted in the steady-state mode using the 9- and 4-mm-diameter orifices (c.f. Table 1) with a flow of N_2O_5 on the order of 1×10^{13} molecules s^{-1}. On sodium chloride flats, we find that $\gamma_1 = (4.0 \pm 2.0) \times 10^{-4}$, on the basis of two experiments, i.e., about a factor of 50 smaller than observed on the NaCl powder. For reaction 6, we find that $\gamma_6 = (4.0 \pm 2.0) \times 10^{-3}$ (six experiments). Again, the uptake is reduced by an order of magnitude relative to that for the powder study. An interpretation of these results is found in the Discussion.

The reason for the large increase in reactivity upon depolishing of the salt flat may be due to the introduction of a distribution of crystal faces. A relevant observation is given by Berko et al.,[7] who report that, in the reaction of $ClONO_2$ with NaBr, visual inspection of the salt crystals showed that different crystal faces may have participated in the chemical reaction to different extents. Although no attempts were made to determine the total surface area of the depolished window, it is unlikely that the available surface increases by a factor large enough to explain the discrepancy on the basis of this effect alone. The lack of reactivity is certainly not due to surface saturation; at the low flow rates employed in these experiments, it would require many tens of seconds of 100% adsorption to form a single monolayer of N_2O_5.

(2) Spray-Coated Surfaces. By spray coating glass optical flats, we intended to obtain a thin, polycrystalline substrate whose total exposed surface is given by the area of the flat. Initially, saturated water solutions of salt were deposited using an atomizer. By scanning electron microscope analysis, these surfaces are found to be poorly reproducible with varying degrees of granularity and porosity. The initial rate of N_2O_5 uptake on these surfaces varies by a factor of 100 and seems to be a function of the substrate thickness. For water-deposited KBr substrates, the uptake as a function of the deposition parameters has been studied systematically. These experiments are conducted in the steady-state configuration using the 9-mm orifice. Even in the limit of low-mass samples (≈5 mg deposited onto 20 cm^2 with 50% coverage), we find that the observed uptake coefficient varies between 3 and 20×10^{-3}. These results are not sufficiently reproducible to allow conclusions to be drawn concerning the true value of γ.

A surface of much higher quality is obtained by using methanol as the atomizing solvent. For NaCl and KBr, we were able to obtain 100% coverage of glass supports with 3−10 mg of salt dispersed over 20 cm^2, resulting in typical thicknesses of 2−8 μm. SEM imaging reveals that these surfaces are nonporous and smooth (c.f. Figure 5). The images shown are those of control samples, prepared simultaneously in batch with the experimental substrate. The SEM analysis allows us to discard samples whose actual exposed surface is estimated to be much greater than the geometrical surface area (by ∼50%). The uptake of N_2O_5 is studied on these surfaces in the steady-state mode using the 4-mm and 9-mm orifices with the flow of N_2O_5 kept as small as possible (about 1×10^{13} molecule s^{-1}). The uptake kinetics on these samples are more reproducible, and γ does not correlate with the deposition thickness. Six experiments on methanol-deposited KBr have been conducted, with surfaces ranging in thickness from 2 to 10 μm, resulting in $\gamma_6 = (3.0 \pm 1.5) \times 10^{-3}$. Three experiments are conducted on NaCl substrates, yielding $\gamma_1 = (5.0 \pm 2.0) \times 10^{-4}$. In both cases, the values are in accord with those determined using the depolished window faces.

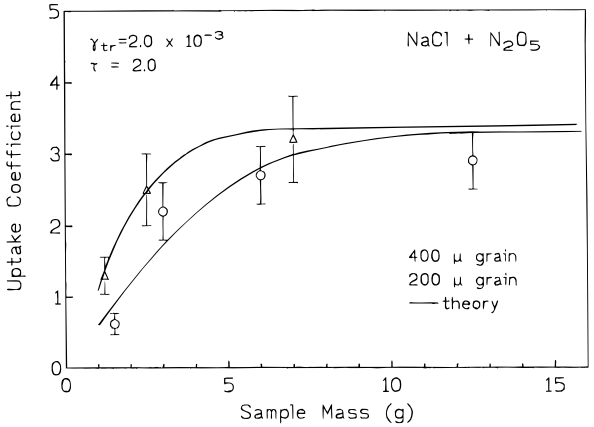

Figure 8. Sample-mass dependence of the N_2O_5 uptake coefficient in units of 10^{-2} on monodisperse NaCl grain. Triangles and circles represent experimental results on 200 and 400 μm grain, respectively. For the implications of the falloff in reactivity at low sample mass, see text. For 400 μm grain, 10 g corresponds to 9.2 layers.

(c) Other Surfaces. *(1) Finer Powder.* A small number of experiments are conducted on KBr powder selected for a finer sieve fraction ($\phi < 10$ μm). This material is about 25% less dense than the powder employed in the product study. In three steady-state experiments, we found that $\gamma_6 = (9.6 \pm 2.0) \times 10^{-2}$, corresponding to a factor of 2 increase compared to that for the coarser powder (c.f. Table 3). The reduced density of the smaller sieve fraction implies that it is characterized by a larger internal void; the subject of diffusion into this interstitial space is taken up in the Discussion.

(2) Monodisperse Sub-millimeter Grain. Additional experiments are conducted using monodisperse grain, in which the reactivity is characterized as a function of the depth of the sample. Because salt crystals are nonporous, as revealed by BET analysis, the total exposed surface of the sample can be determined from the geometrical surface area of the grains. Before each experiment, the salt grain is weighed and leveled into a flat-bottomed sample dish ($\phi = 50$ mm). With the known diameter of the salt crystals, we can calculate the effective number of grain layers for a given sample mass. With the additional information of the bulk density, measured volumetrically for each sample, we have all the necessary information to calculate the appropriate correction factor by the procedure outlined by Keyser and co-workers.[26−28] The uptake of N_2O_5 is characterized for each of a series of sample masses covering the range of one to ten effective salt crystal layers. The experiments are carried out in the steady-state mode, using the 9-mm orifice under small N_2O_5 flows (flow $< 1 \times 10^{13}$ molecules of N_2O_5 s^{-1}). The results of these experiments are shown in Figures 8 and 9. For each reaction, the uptake is measured as a function of sample mass for two grain sizes. Although the uncertainty of an individual uptake measurement is large (20%), the observed uptake clearly decreases at low sample mass and demonstrates a small grain-size dependence. This is in good agreement with the reactivity anticipated by the treatment of Keyser et al., shown as solid lines in the figures.

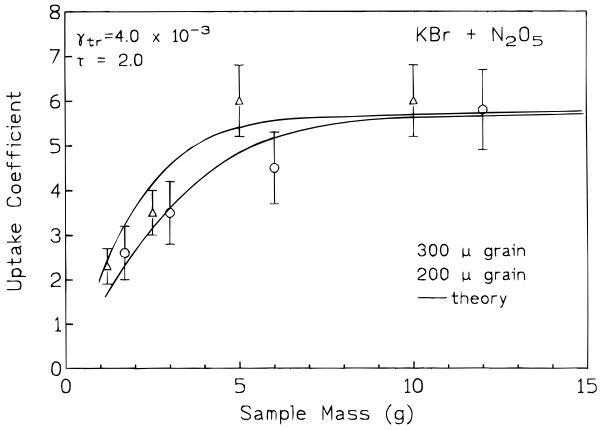

Figure 9. Uptake coefficient in units of 10^{-2} versus sample mass for the N_2O_5 uptake on monodisperse KBr grain. Triangles and circles represent experiments conducted with 200 and 300 μm grain, respectively. For 300 μm grain, 10 g corresponds to 12.3 layers.

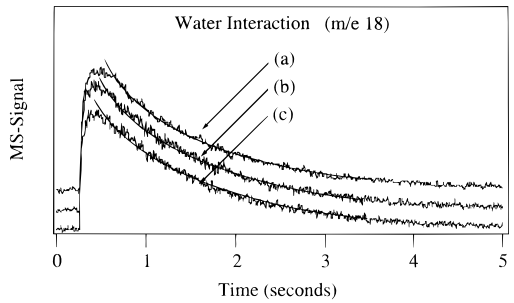

Figure 10. Pulsed-valve traces (recorded at *m*/*e* 18) of 1×10^{15} molecules of water to study its interaction with KBr powder (prepared as for the product study) under the following conditions: (a) a control pulse of H_2O is added to the reactor with the sample-isolation plunger closed; (b) a second pulse is injected with the KBr powder exposed; and (c) a third pulse is introduced during an N_2O_5 exposition to the KBr powder, i.e., while reaction 6 is in course. Under all conditions, the H_2O profile is characterized by its rate of effusive loss from the cell, indicating no additional loss process for H_2O.

The details and implications of the agreement are presented in the Discussion.

(d) Role of Humidity. Because we are concerned with the applicability of our experimental findings for atmospheric chemistry, it is important to study the influence of water vapor on the kinetics of reactions 1 and 6. Gas-phase water concentrations cannot be raised to atmospherically relevant levels inside the Knudsen reactor, but we are able to obtain some information concerning the water interaction with the reactive systems under study by (1) heating the solid sample to eliminate traces of humidity in the salt sample and by (2) adding water concurrently with N_2O_5 to see the effect on the kinetics and the product yields. The maximum gas-phase water concentration presently attainable is on the order of 10^{13} molecule cm^{-3}. In Figure 10, we show the results of a series of pulsed valve experiments in which 1×10^{15} molecules of water are introduced into the cell (yielding a maximum density of 5×10^{12} cm^{-3}) under three conditions: (a) The salt sample (NaCl powder) is isolated with the plunger sealing off the sample chamber; (b) H_2O is pulsed into the cell in the presence of the salt; (c) H_2O is pulsed into the reactor during the reaction of N_2O_5 with NaCl. All three traces are characterized by the rate of effusion of H_2O from the reactor. On the basis of this and similar experiments, we find no evidence for any interaction of gaseous water with the reactive systems under study over the range of attainable water densities and on the time scale of the experiment.

TABLE 4: Experimental Results: NaCl and KBr with HNO_3

substrate	γ_{obs} (NaCl)[a]	expt	γ_{obs} (KBr)[a]	expt
(1) powder (35−160 μm)	2.8 ± 0.5	20	2.8 ± 0.5	5
(2) grain (300 μm)			4.7 ± 0.6	5
(3) spray-coated sample	2.2 ± 1.0	1	1.7 ± 0.8	1
(4) polished window face	1.3 ± 0.6	2	0.5 ± 0.3	1
(5) depolished window face	5.5 ± 2.0	2	2.6 ± 1.3	1

[a] γ values are in units of 10^{-2}. See text for discussion of uncertainty. The recommended value cited in the text weighs most heavily the results for substrates 3 and 5.

With the use of the heatable sample holder, we have studied the effect of the *absence* of residual water vapor in the salt samples. We have already described the change in the product spectrum that is observed for reaction 6 when fully dried KBr substrates are exposed to N_2O_5. The uptake of N_2O_5 on NaCl is slow, and the 20-cm^2 total surface of the heatable sample holder is insufficient to study this effect for reaction 1. Because the heatable sample holder has been constructed since our publication on reactions 2 and 7, we briefly describe here the effect of drying salt substrates with respect to HNO_3 reactivity. The NaCl optical flats heated under vacuum for several hours demonstrate the same reactivity as those that are not dried. In the previous study,[2] we report that added water vapor does not change the observed kinetics of reactions 2 and 7. Thus, over the range of conditions available to our experimental technique, from extremely dried samples (in the presence of 10^{10} cm^{-3} of background H_2O) to about 10^{13} cm^{-3} of gaseous water, we observe no change in the uptake kinetics for the HNO_3 and N_2O_5 reactions studied. The degree to which the sample is dried does determine whether HONO is observed as a product of reaction 6, as described above.

(1) Additional Experiments with HNO_3. In a recent study on the reactions of HNO_3 with salt powder,[2] we reported that, for all the salts examined, the uptake coefficient could be described as $\gamma = (2.8 \pm 0.5) \times 10^{-2}$, a value close to that found here for the interaction of N_2O_5 with salt powders. Unlike the N_2O_5 reactions, the uptake coefficient γ_2 was found to depend only on the geometrical cross section presented by the sample dish in which the powder was placed. Notably, the uptake coefficient did not depend on the degree of sample-dish filling or on the extent to which the salt was milled, implying that diffusion into the internal void of the powder does not contribute to the observed uptake for this reaction. With evidence for a strong dependence of the N_2O_5 uptake on the sample preparation, we decided to conduct additional experiments to better characterize this effect for the uptake of HNO_3 on salt. We exposed HNO_3 to (1) polished salt windows, (2) depolished salt windows, (3) thin spray-coated surfaces, and (4) monodisperse grains. The results of these experiments are summarized in Table 4. In general, the HNO_3 uptake is not enhanced by the presence of an internal void. This is demonstrated most convincingly in Figure 11, where the uptake of HNO_3 on KBr monodisperse grain (300-μm diameter) is shown as a function of sample mass. Unlike in the N_2O_5 experiments (c.f. Figures 8 and 9), no mass dependence is observed as the effective number of grain layers decreases to unity.

4. Discussion

In this study, we elucidate the physical−chemical phenomena involved in the heterogeneous interaction of N_2O_5 and HNO_3 with salt and quantify the rate constants from which a reaction probability can be determined. For atmospheric applications, the salt samples employed in the experiments can be considered

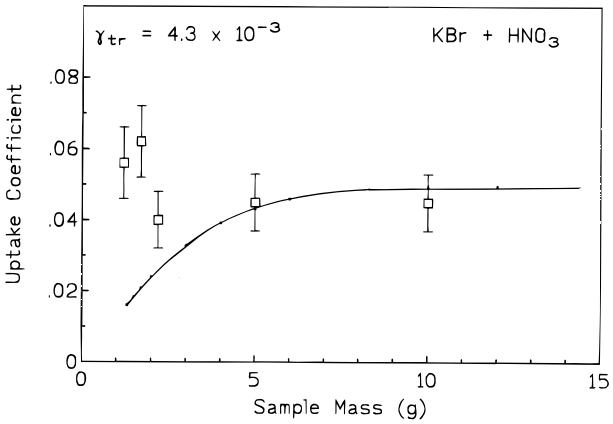

Figure 11. Observed rate of uptake versus sample mass for the HNO_3 reaction on KBr monodisperse grain of 300 μm diameter. Experimental results are presented by open squares. No reduction in reactivity is observed for low-mass samples, in stark contrast to the N_2O_5 uptake on the same material. The theoretical curve is calculated to be in agreement with the limit of large sample mass. Here, 10 g correspond to 12.3 layers.

as "model" substrates; i.e., the applicability of this study to atmospheric chemistry depends on the extent to which the solid reactant represents the salt emitted into the atmosphere. Powders, grains, or spray-deposited surfaces, even after correction for the effect of diffusion into the internal void, may each reflect to a different degree the reactivity of dry sea-salt aerosol. For example, the probability of any given gaseous species reacting with salt may depend on the crystal face distribution, as discussed in the previous section. Differently prepared samples may reveal different values for the uptake coefficient due to this effect.

Our principal experimental results can be summarized by the following points: (1) On powders, N_2O_5 reacts with high uptake probability with NaCl and KBr; the main reaction products are $ClNO_2$ (60% yield) and Br_2 (35% yield), respectively. (2) On samples prepared to eliminate diffusion into the internal void, the uptake of N_2O_5 is reduced by more than a factor of 10. (3) With sub-millimeter monodisperse crystals, a sample-mass dependence on the uptake rate is observed. (4) On fine KBr powders ($\phi < 25$ μm), the uptake of N_2O_5 is enhanced relative to that for the powder selected for the product study. (5) Water plays no significant role in the rate of uptake of N_2O_5 over the range of H_2O partial pressures that is attainable by our experimental technique. (6) HNO_3 reactivity is not enhanced by samples prepared with a large internal void (grains and powders).

Before we begin the treatment of the kinetic data, we comment briefly on the product spectra of the reactions under study. Reaction 1 has been reported to produce $ClNO_2$ as the sole gas-phase chlorine-containing species at relative humidities below the deliquescence point.[12,15] All our experimental results are in accord with this conclusion. The less-than-unity yield for $ClNO_2$ is in stark contrast to the HNO_3 reaction with salt under the same conditions, where a one-for-one conversion of HNO_3 to HCl has been observed.[2] For reaction 1, one or more secondary processes may exist; for example, N_2O_5 might bind to dry salt in a state that does not immediately react to yield $ClNO_2$, or a fraction of the N_2O_5 may be hydrolyzed to form adsorbed nitric acid.

The more surprising result concerns the formation of Br_2 as the sole gas-phase bromine-containing species from the reaction of N_2O_5 with KBr. Finlayson-Pitts et al. give evidence for the direct formation of $BrNO_2$ in reaction 6 under very different experimental conditions.[24] In their experiment, a few hundred millitorr of N_2O_5 is reacted with 100 g of NaBr under an atmosphere of helium. The reacting mixture is expanded into a halocarbon-wax-coated IR cell, again pressurized to an atmosphere of helium. It is possible that they observe some $BrNO_2$ yield because the high pressure of helium efficiently reduces the gas-phase diffusion rate of the $BrNO_2$ product to the bromide. Clearly, this reaction needs to be investigated further to determine the conditions under which Br_2, HONO, and $BrNO_2$ are produced in significant yield, including over the range of relative humidities that are relevant to atmospheric chemistry.

The observation of Br_2 from reaction 6 suggests that the chemical nature of $BrNO_2$ is different from that of $ClNO_2$, which is stable in the presence of chloride under the same conditions. From heats of formation,[25] it is found that the reaction of gaseous $BrNO_2$ with KBr to yield Br_2 is slightly exothermic, whereas the analogous reaction between $ClNO_2$ and chloride to give Cl_2 is about 40 kJ mol^{-1} endothermic. However, if bromide can be oxidized efficiently to bromine by reaction 8, as is suggested by the experimental evidence, this would imply that the Br atom in $BrNO_2$ is in the (+I) oxidation state. Thus, $BrNO_2$ might best be considered as the N(+III) mixed-acid anhydride of HOBr and HONO; in contrast, $ClNO_2$ is the N(+V) mixed-acid anhydride of HCl and HNO_3.

Our quantitative determination of the uptake coefficients relies mostly on the experiments conducted on the spray-coated flats and on the monodisperse crystals; in the former, we can inspect the samples directly by SEM techniques to ensure that the exposed surface is of high quality, and in the latter the total exposed surface of the samples can be calculated from the known geometry of the crystals. To understand the ensemble of our experimental results, the enhancement of reactivity by diffusion into the internal void must be considered. The discussion is guided by the treatment proposed by Keyser and co-workers for the reactivity of porous substrates;[26−28] for details of the calculations, the reader is referred to those references and to the original derivations, described by Aris, Wheeler, and others.[32,33] The equations used for the correction factors calculated below can be found in Table 5.

The discussion begins with the definition of the Thiele modulus, which is defined as the following function of k, the first-order heterogeneous rate constant, and D, the diffusion constant of the gas within the porous solid:

$$\phi = h(k/D)^{0.5} \qquad \text{(eq 2)}$$

where h is a length related to the thickness of the substrate. The simplest case to consider, and the one that corresponds to our experimental conditions, is that where the mean free path of the gas molecules is much longer than the typical pore diameter. This allows the use of the Knudsen diffusion coefficient, which can be calculated knowing only the molecular weight of the gas species and the geometrical constraints of the substrate (c.f. Table 5). The calculation is carried out assuming ideal cylindrical pores; a tortuosity factor, τ, is then introduced to take into account the real pore geometry. In a sense, the use of well-characterized salt grains provides an ideal test for the applicability of the theory of porous solid reactivity because, in this case, the "pores" are just the interstitial spaces between the grains. With certain simplifications concerning the size and shape of the particles and the nature of the packing, we can write an expression for the Thiele modulus in terms of the sample density, the tortuosity factor, and the "true" value of the uptake coefficient, γ_{tr}. The calculation of a correction factor thus consists of the following steps: (1) The number of layers, N_L, and height of the sample, h_i, is determined knowing

TABLE 5: Parameters Used in Correction Factor Calculation

parameter	value	notes
τ	2.0	value determined by best fit to data
grain diameter, NaCl	400, 200 μm	sieved and analyzed by SEM
grain diameter, KBr	300, 200 μm	sieved and analyzed by SEM
γ_{tr}, NaCl	2.0×10^{-3}	best fit to experimental data
γ_{tr}, KBr	4.0×10^{-3}	best fit to experimental data
ρ_b, NaCl	1.35 g cm^{-3}	measured volumetrically
ρ_t, NaCl	2.16 g cm^{-3}	ref 31
ρ_b, KBr	1.60 g cm^{-3}	measured volumetrically
ρ_t, KBr	2.75 g cm^{-3}	ref 31

Equations Used in Analysis (See Text for Definition of Variables)

simple cubic packing	hexagonal close packed
(1) $h_i = d(N_L - 0.5)$	$h_i = d[(N_L - 1)(2/3)^{0.5} + 0.5]$
(2) $\phi = (h_i/d)\,[3\rho_b/2(\rho_t - \rho_b)](3\tau\gamma_{tr})^{0.5}$	same
(3) $\eta = \frac{1}{\phi}\tanh\phi$	same
(4) $\gamma_{obs} = (\pi/2)[1 + \eta(2N_L - 1)]\gamma_{tr}$	$\gamma_{obs} = (\pi/\sqrt{3})[1 + \eta[2(N_L - 1) + (3/2)^{0.5}]]\gamma_{tr}$

Other Relations

$$D_e = \frac{2\Theta r_p \upsilon}{3\sigma}$$

where D_e = Knudsen diffusion coefficient
Θ = porosity, defined as $1 - (\rho_b/\rho_t)$
r_p = the pore radius
υ = molecular velocity
τ = tortuosity factor

the bulk density of the powder, the area of the sample holder, and the mass of the sample. (2) The Thiele modulus is calculated assuming γ_{tr} and τ. (3) The "effectiveness" parameter, η, defined as the degree to which the underlayers of grain contribute to the overall uptake, is calculated. (4) The correction factor is determined and applied to the assumed γ_{tr}. The theoretical curves shown in Figures 8 and 9 are derived by finding the values of γ_{tr} and τ that give the best agreement with the experimental data.

The sieved powders are characterized by a distribution of grain diameters, so the correction-factor calculation for these substrates can be carried out only semiquantitatively. This complication is somewhat avoided because enough powder is present in these experiments so that the correction is calculated for the limit of many grain layers. When N_L is large (>5), the correction factor is far more sensitive to the bulk density of the powder than the diameter of the grains. Using $\tau = 2$ (see below), the theory yields values for γ_{tr} that are more than an order of magnitude smaller than those experimentally observed. The results of the calculations are summarized in Tables 2, 3, and 5. The appropriate correction factor for the powders used in the product study is on the order of 20 for NaCl and 15 for KBr, which would yield the values $\gamma_1 = 1.7 \times 10^{-3}$ and $\gamma_6 = 3.5 \times 10^{-3}$. When the same calculation is carried out for the powder sieved for diameters less than 25 μm, an even larger value for the correction factor is obtained (c.f. Table 3).

A more rigorous test of the theory is found in the experiments conducted with the monodisperse grains. With this material, we can better characterize the total exposed surface area, and because the grains are macroscopic, it is easy to prepare the sample to assure homogeneous spreading across the sample holder. Using $\tau = 2.0$ in the correction-factor calculation, which is the value suggested by Timonen et al. in their recent study of $ClONO_2$ on NaCl,[13] we find remarkably good agreement for the four sets of data. The values of γ_{tr} that yield the best fits to the experimental results are $\gamma_{tr} = 2.0 \times 10^{-3}$ for reaction 1 and $\gamma_{tr} = 4 \times 10^{-3}$ for reaction 6. The theory not only correctly reproduces the dependence on sample mass but also confirms the observation that the kinetic limit of many grain layers is attained at lower sample mass for smaller grain size. The assessment of the uncertainty for these determinations is difficult; when large correction factors (>10) are applied to experimentally obtained values to obtain "true" values, the methods should be considered approximate. However, the result offers strong evidence that diffusion into the internal void of the powder and grain samples is contributing to the overall uptake kinetics and that the treatment of Keyser and co-workers is applicable to the reactions of N_2O_5 on salt.

TABLE 6: Summary of This and Previous Work on Reaction 1

ref	technique	γ_{obs} (NaCl)	RH
11	static reactor	$>2.5 \times 10^{-3}$	0%
13	aerosol reactor	$(3.0 \pm 0.2) \times 10^{-2}$	71−92%
14	aerosol reactor	"small"	50%
15	annular tube reactor	1.0×10^{-3}	45−96%
this work	Knudsen cell	5.0×10^{-4}	0%

The uptake coefficients determined from spray-coated samples and window faces can be compared directly to the corrected γ determined from monodisperse grain. The results are summarized in Tables 2 and 3. It can be seen that, for reaction 6, all measurements are in good agreement, with $\gamma_6 = (4.0 \pm 1.0) \times 10^{-3}$. For the NaCl substrates, the uptake coefficient determined from spray-coated and window surfaces is a factor of 4−5 smaller than the value extrapolated from monodisperse grain experiments. There are several possible reasons for this discrepancy, including (1) significantly different distributions of crystal faces among the sample types, (2) differences in the external surface area, (3) imprecision in the extrapolation of the observed to "true" values of γ for the monodisperse grain samples, or (4) variations in the surface water content for the various substrates. With these various considerations in mind, we prefer the lower, directly determined values of $\gamma_1 = (5.0 \pm 2.0) \times 10^{-4}$.

The summary of this and previous work is given in Table 6. Our value for γ_1 is smaller than expected on the basis of the previous studies of the reaction. The lower limit to γ_1 estimated

by Livingston and Finlayson-Pitts, to our knowledge the only previous study of reaction 1 on dry salt, is a factor of 5 larger than the γ_1 we report. It is interesting to note that their value is in agreement with our determination of γ_1 on the basis of the monodisperse grain study. Behnke and co-workers limit their kinetic measurements to relative humidities above 72%, the deliquescence point of NaCl; their results are therefore not directly comparable to ours. However, they have some experimental data at 50% relative humidity,[15] where they find qualitatively that the uptake coefficient is much smaller than the value they determine above 72% relative humidity. The evidence is mounting that at least two values of the uptake coefficient are needed to describe the atmospheric interaction of N_2O_5 with NaCl: a large value for aerosols humidified above the deliquescence point and a much smaller value for the direct reaction with "dry" salt. It is under conditions of low relative humidity that our experimentally determined values of the uptake coefficient apply.

It is pertinent to note that a humidity effect on the uptake of N_2O_5 by aerosols has been suggested by Platt and co-workers[3] to explain some of their *in-situ* observations on the nitrate radical, NO_3. The main loss of the nitrate radical in the nighttime troposphere is thought to occur indirectly via the heterogeneous loss of N_2O_5:

$$NO_2(g) + NO_3(g) \leftrightarrow N_2O_5(g) \qquad (11)$$

$$N_2O_5(g) + H_2O(ads) \rightarrow 2HNO_3(ads) \qquad (9)$$

When they plot their NO_3-concentration data as a function of relative humidity registered at the time of the measurement, they find abrupt downward transitions in nitrate radical concentration at relative humidities that correspond to the deliquescence points of sulfate salts. This observation is evidence that the N_2O_5 uptake coefficient also changes abruptly at deliquescence points.

The new kinetic measurements on the HNO_3 reactions with NaCl and KBr demonstrate that, in stark contrast to reactions 1 and 6, diffusion into the internal void contributes little to the total rate of nitric acid adsorption. Even with the large variation of sample preparation, we observe a value for the uptake coefficient on the order of $\gamma = 3 \times 10^{-2}$. The exception is again the polished window face, which is less reactive than the other substrates. Of particular interest are the five experiments conducted on the KBr monodisperse grain (c.f. Figure 11), where no variation in the rate of uptake is observed as a function of the total sample mass.

Our earlier observations, that the rate of HNO_3 uptake depends only on the external geometrical surface area, is confirmed. Thus HNO_3 reactivity does not follow the behavior predicted by the treatment of Keyser et al.; according to the theory, if an observed uptake coefficient is 10^{-2} on grains and powders, then the associated correction factor that needs to be applied to obtain the "true" uptake coefficient is large ($\sim$10). Indeed, the similar rates of uptake of HNO_3 and N_2O_5 on powders ($\gamma_{N_2O_5} = \gamma_{HNO_3} = 10^{-2}$) and the very different uptake rates on substrates without an internal void ($\gamma_{HNO_3} \approx 10^2\, \gamma_{N_2O_5}$) reveal that distinct mechanisms are at play for each process. The physical−chemical assumptions of the correction-factor calculation appear to adequately describe the N_2O_5 interaction with salt; the HNO_3 interaction appears to be different.

An hypothesis to explain the observations is that HNO_3 diffusion into the bulk of a granular substrate is much slower than predicted by the relevant equations given in Table 5; i.e., HNO_3 is behaving as a "sticky" molecule. Because our experiment measures the rate of *irreversible uptake* of a gaseous species, it is possible to have a compound that is "sticky" and characterized by a small reaction probability. The following simple kinetic model is used to illustrate this point:

$$HNO_3(g) \underset{-1}{\overset{1}{\rightleftharpoons}} HNO_3(ads) \overset{2}{\rightarrow} HNO_3(reac)$$

In this picture, an adsorbed state is formed on every collision (k_1 = collision frequency, ω). The lifetime of HNO_3(ads) with respect to desorption is given by $1/k_{-1}$, and k_2 is the first-order rate constant for the formation of a reactive state, from which the observed reaction begins. The fraction of collisions that yields the reactive state is given by a simple branching-ratio expression, $F = k_1k_2/(k_2 + k_{-1})$. In this picture, the "stickiness" of a molecule is determined by the magnitude of k_{-1} relative to k_{esc} (i.e., relative to the time scale of our experiment). The rate of diffusion into the interstitial void will be unimportant if the lifetime associated with the adsorbed state becomes long relative to k_2, the rate of reaction. With the experimental observation of the overall kinetics of disappearance from the gas-phase, we have no means of obtaining independent values for k_{-1} and k_2. In our previous modeling of reaction 2, we assigned a single rate constant to represent the rate of formation of the reactive precursor. The existence of a precursor to the reactive state for "sticky" molecules would explain the reduced role of diffusion with respect to reaction and, by extension, the failure of the treatment of Keyser et al. to describe the experimental observations.

To fit the observed sample-mass dependence for reaction 2 using the correction-factor calculation (c.f. Figure 11), we need to reduce the value of the diffusion constant by two orders of magnitude. The reduced rate of diffusion results in correction factors that are less than 2.5 even for the finest powders studied, although it is questionable whether the correction factors thus obtained are meaningful. On the basis of these new and our previous experiments[2] on the reaction of HNO_3 with salt, we recommend the value $\gamma_2 = (2.0 \pm 1.0) \times 10^{-2}$. In particular, we place emphasis on the experimental results from samples prepared to eliminate the effects of diffusion into the internal void. The broader error estimate takes into account the variations observed over the range of experimental conditions studied. This value is two orders of magnitude greater than one recently reported by Laux et al.[6] They conducted experiments on a NaCl single crystal, cleaved in the (100) orientation, mounted in a vacuum chamber, and subject to a flow of nitric acid from a capillary. By X-ray photoelectron spectroscopy, the rate of nitrate formation on the crystal surface is monitored; this rate is then related to an uptake coefficient by assuming that the saturation point for nitric acid exposure corresponds to the formation of one monolayer of nitrate. A contributing factor to the lower reactivity they observe may be the use of a single crystal face—we find also that polished salt flats are at least a factor of 5 less reactive than the other substrates studied with respect to reaction with N_2O_5 and HNO_3. To resolve these questions, it would be of interest to cleave salt crystals to expose faces of higher Miller index to study the relationship between crystal orientation and reactivity.

Our uptake measurements provide a novel perspective to the debate on the need to apply correction factors to data obtained on "porous" substrates. Our results show that they may or may not be needed, depending on the diffusion properties of the gaseous reactant into and within the internal void of the solid substrate. If it can be shown that Knudsen diffusion is a good description of this process, then the correction scheme offered by Keyser and co-workers provides a means of taking the effect into account. Unfortunately, many gases of atmospheric interest, such as HNO_3, H_2O, H_2O_2, and $ClONO_2$ are known to

experimentalists as "sticky" compounds with respect to their interactions with the walls of reactors. This behavior may be an indication that their respective diffusion coefficients on many types of materials, including salt, may deviate significantly from the value determined from the molecular weight (i.e., the Knudsen relationship).

In the Introduction, we consider several reactions between nitrogen oxides and salt that may liberate gaseous chlorine-containing species into the Earth's atmosphere. We find in this study that the reaction between N_2O_5 and salt is slow in the absence of water, information that may be of use for chemical modeling of the dry atmosphere (e.g., the stratosphere after volcanic eruption or the winter troposphere at high latitudes). Since the reaction of HNO_3 with NaCl is at least an order of magnitude faster under the same conditions, the production of HCl is likely to be greater than that of $ClNO_2$, the photolyzable product of reaction 1. Unfortunately, no data exist concerning the uptake efficiencies of nitric acid on salt humidified above the deliquescence point. Although a full understanding of the relative roles of reactions 1−4 in atmospheric chemistry will be available only after the relative-humidity dependence of these processes is elucidated, our results can be used as a lower limit to the true uptake coefficients for relative humidities below the deliquescence point. Another result with potentially interesting implications is our observation of Br_2 and HONO products from the reaction of N_2O_5 with KBr and NaBr. If the reaction is favored under certain local situations, such as those encountered in the formation of the "arctic" tropospheric ozone hole,"[36] then it may represent a non-negligible source of photolytic bromine and nitrous acid.

5. Summary and Conclusions

The significant findings of this work can be summarized in three points: (1) The reaction of N_2O_5 on dry NaCl is found to be slower than previously thought, highlighting the need for uptake coefficient data over a range of relative humidities for use in atmospheric modeling. The study confirms that $ClNO_2$ is the product of the reaction. (2) The reaction of N_2O_5 with KBr takes place with greater reaction probability than the corresponding NaCl reaction, and the only gaseous bromine-containing species observed under our conditions is Br_2. We propose a redox process in which the oxidation of Br^- to bromine is accompanied by the reduction of nitrate to nitrite, which, upon acidification, is released as nitrous acid. (3) The role of internal surfaces in the overall observed uptake kinetics for the reactions of N_2O_5 is found to be remarkably well described by the treatment given by Keyser and co-workers. Additional experiments on the uptake kinetics of nitric acid, however, cast doubt that this treatment can be generally extended to all species of atmospheric interest. This is important because granular substrates are often employed in the study of heterogeneous reactivity. To elucidate the nature of heterogeneous processes, it is important, as Keyser et al. have stressed, to work with well-characterized substrates; it appears now that one must, in addition, design experiments to characterize the diffusion properties of the gaseous reactant if the substrate is "porous". (4) Our rate measurements will be useful for the modeling of natural events in which salt comes into contact with the dry atmosphere.

Acknowledgment. Funding for this work was provided by the Office Fédéral de l'Education et de la Science (OFES) as part of the HALIPP subproject of the EUROTRAC program and by the Fonds National de la Recherche Scientifique (FNRS) under Grant No. 20-37599.93. We thank Professor Hubert van den Bergh for his lively interest and input.

References and Notes

(1) Finlayson-Pitts, B. J.; Pitts, J. N. *Atmospheric Chemistry*; John Wiley and Sons: New York, 1986.

(2) Fenter, F. F.; Caloz, F.; Rossi, M. J. *J. Phys. Chem.* **1994**, *98*, 9801.

(3) Platt, U.; Hausmann, M. *Res. Chem. Intermed.* **1994**, *20*, 577.

(4) Harrison, R. G.; Msibi, M. I.; Kitto, A.-M. N.; Yakulki, S. *Atmos. Environ.* **1994**, *28*, 1593.

(5) Woods, D. C.; Chuan, R. L.; Rose, W. I. *Science* **1985**, *230*, 170.

(6) Laux, J. M.; Hemminger, J. C.; Finlayson-Pitts, B. J. *Geophys. Res. Lett.* **1994**, *21*, 1623.

(7) Berko, H. N.; McCaslin, P. C.; Finlayson-Pitts, B. J. *J. Phys. Chem.* **1991**, *95*, 6951.

(8) Vogt, R.; Finlayson-Pitts, B. J. *J. Phys. Chem.* **1994**, *98*, 3747.

(9) Finlayson-Pitts, B. J. *Nature* **1983**, *306*, 676.

(10) Finlayson-Pitts, B. J.; Johnson, S. N. *Atmos. Environ.* **1988**, *22*, 1107.

(11) Finlayson-Pitts, B. J.; Ezell, M. J.; Pitts, J. N. *Nature* **1989**, *337*, 241.

(12) Livingston, F. E.; Finlayson-Pitts, B. J. *Geophys. Res. Lett.* **1991**, *18*, 17.

(13) Timonen, R. S.; Chu, L. T.; Leu, M.-T.; Keyser, L. F. *J. Phys. Chem.* **1994**, *98*, 9509.

(14) Behnke, W.; Krueger, H.-U.; Scheer, V.; Zetzsch, C. In *Proceedings of the EUROTRAC Symposium '92*; Borrell, P. M., Ed.; SPB Academic Publishing: The Hague, The Netherlands, 1993.

(15) Behnke, W.; Zetzsch, C. *J. Aerosol. Sci.* **1990**, *21* (*Suppl. 1*), S229.

(16) Msibi, I. M.; Li, Y.; Shi, J. P.; Harrison, R. M. *J. Atmos. Chem.* **1994**, *18*, 291.

(17) Parrish, D. D.; Hahn, C. J.; Williams, E. J.; Norton, R. B.; Fehsenfeld, F. C.; Singh, H. B.; Shetter, J. D.; Gandrud, B. W.; Ridley, B. A. *J. Geophys. Res.* **1993**, *98* (D8), 14995.

(18) Finlayson-Pitts, B. J.; Livingston, F. E.; Berko, H. N. *Nature* **1990**, *343*, 622.

(19) Chameides, W. L.; Stelson, A. W. *J. Geophys. Res.* **1992**, 97 (D18), 20565.

(20) Pszenny, A. A. P.; Keene, W. C.; Jacob, D. J.; Fan, S.; Maben, J. R.; Zetwo, M. P.; Springer-Young, M.; Galloway, J. N. *Geophys. Res. Lett.* **1993**, *8*, 699.

(21) Keene, W. C.; Pszenny, A. A. P.; Jacob, D. J.; Duce, R. A.; Galloway, J. N.; Schultz-Tokos, J. J.; Sievering, H.; Boatman, J. F. *Global Biogeochem. Cycles* **1990**, *4*, 407.

(22) Singh, H. B.; Kasting, J. F. *J. Atmos. Chem.* **1988**, *7*, 261.

(23) Michelangeli, D. V.; Allen, M.; Yung, Y. L. *Geophys. Res. Lett.* **1991**, *18*, 673.

(24) Finlayson-Pitts, B. J.; Livingston, F. E.; Berko, H. N. *J. Phys. Chem.* **1989**, *93*, 4397.

(25) All thermodynamic data are taken from "The NBS tables of chemical thermodynamic properties" [*J. Phys. Chem. Ref. Data* **1982**, *11* (*Suppl 2*)], except for those for $BrNO_2$, which are taken from ref 34.

(26) Keyser, L. F.; Moore, S. B.; Leu, M.-T. *J. Phys. Chem.* **1991**, *95*, 5496.

(27) Keyser, L. F.; Leu, M.-T.; Moore, S. B. *J. Phys. Chem.* **1993**, *97*, 2800.

(28) Chu, L. T.; Leu, M.-T.; Keyser, L. F. *J. Phys. Chem.* **1993**, *97*, 12798.

(29) Tabor, K.; Gutzwiller, L.; Rossi, M. J. *J. Phys. Chem.* **1994**, *98*, 6172.

(30) Müller-Markgraf, W.; Rossi, M. J. *Rev. Sci. Instrum.* **1990**, *61*, 1217.

(31) Ganske, J. A.; Berko, H. N.; Finlayson-Pitts, B. J. *J. Geophys. Res.* **1992**, *97* (D7), 7651.

(32) Aris, R. *The Mathematical Theory of Diffusion and Reaction in Permeable Catalysts*, Vol. *1*, *The Theory of the Steady State*; Clarendon Press: Oxford, 1975.

(33) Wheeler, A. *Adv. Catal.* **1951**, *3*, 249.

(34) Kreutter, K. D.; Nicovich, J. M.; Wine, P. H. *J. Phys. Chem.* **1991**, *95*, 4020.

(35) *C.R.C. Handbook of Chemistry and Physics*, 55th ed.; CRC Press: Cleveland, OH, 1974.

(36) McConnell, J. C.; Henderson, G. S.; Barrie, L.; Bottenheim, J.; Niki, H.; Langford, C. H.; Templeton, E. M. J. *Nature* **1992**, *355*, 150.

JP9503829